High temperature properties of the monolithic CVD β-SiC materials joined with a pre-sintered MAX phase Ti_3SiC_2 interlayer via solid-state diffusion bonding – Accepted 04.11.16

*Peter Tatarko[a], Zdeněk Chlup[b], Amit Mahajan[a], Valentina Casalegno[c], Theo G. Saunders[a], Ivo Dlouhý[b], Michael J. Reece[a],

[a]School of Engineering & Materials Science and Nanoforce Technology Ltd., Queen Mary University of London, Mile End Road, London E1 4NS, United Kingdom

[b]Institute of Physics of Materials, Academy of Sciences of the Czech Republic, Žižkova 22, 616 62 Brno, Czech Republic

[c]Politecnico di Torino, Applied Science and Technology Department, Corso Duca degli Abruzzi 24, 10129 Torino, Italy

Abstract

Monolithic high purity CVD β-SiC materials were successfully joined with a pre-sintered Ti_3SiC_2 foil via solid-state diffusion bonding. The initial bending strength of the joints (~ 220 MPa) did not deteriorate at 1000°C in vacuum, and the joints retained ~ 68% of their initial strength at 1200°C. Damage accumulation in the interlayer and some plastic deformation of the large Ti_3SiC_2 grains were found after testing. The activation energy of the creep deformation in the temperature range of 1000-1200°C in vacuum was ~ 521 $kJ.mol^{-1}$. During the creep, the linkage of a significant number of microcracks to form a major crack was observed in the interlayer. The Ti_3SiC_2 interlayer did not decompose up to 1300°C in vacuum. A mild and well-localized decomposition of Ti_3SiC_2 to TiC_x was found on the top

surface of the interlayer after the bending test at 1400°C in vacuum, while the inner part remained intact.

Keywords:

Diffusion joining; SiC; MAX phase; high temperature mechanical properties; spark plasma sintering

1. Introduction

Due to their excellent combination of properties, SiC monolithic and composite materials are primarily used as materials for aerospace and nuclear applications. In addition, SiC based composites are also being developed for aerospace and ground-based engine and hot structure fusion reactor applications [1]. In the nuclear field the most important application of SiC is for cladding materials in pressurised water reactors and flow channel insert materials in thermonuclear fusion reactors [2]. In fission power applications, fully ceramic SiC cladding and ceramic/metal cladding are two generic types of materials currently being considered for light-water reactors [3]. The fully ceramic cladding usually consists of a combination of fibrous SiC composites with a single layer or multiple layers of monolithic SiC coatings [3].

A Chemical Vapour Deposition (CVD) process can be used to produce high-purity, highly crystalline, fully dense (3.21 g/cm^3) stoichiometric β-SiC [4, 5]. CVD SiC has a cubic β-SiC structure while hot-pressed or sintered SiC has the hexagonal α-SiC structure [5]. Among all SiC based materials, CVD β-SiC exhibits the highest elastic modulus and superior irradiation resistance [4]. CVD SiC is considered in aerospace and nuclear applications as a monolithic material or an external coating

on SiC-matrix fibrous composites. In most cases, however, the ability of joining SiC based materials to themselves or other dissimilar materials is a critical technological need for their applications.

Among all of the joining approaches, only a few methods are appropriate for nuclear environment. It has been reported that diffusion bonding is a promising method of joining SiC for nuclear applications [3, 6]. In recent years, Spark Plasma Sintering (SPS) has attracted considerable interest as a new advanced technique for the joining of both monolithic SiC [4, 7, 8, 9] and ceramic matrix composites (CMCs) [10, 11, 12]. In this case, both a rapid heating and a short processing time allow a highly controllable reaction of the interlayer with the materials to be joined [4, 8, 10]. At the same time, the electric field can accelerate self-diffusion, and promote the migration of ions through the joining interface [8].

Apart from the use of the appropriate joining techniques, another critical issue is to develop new joining filler materials with high melting points, good oxidation and irradiation resistance. MAX phases (M is an early transition metal, A is an A-group element, and X is either C or N) are layered ternary materials with a unique combination of metallic and ceramic properties, such as damage tolerance, machinability, high temperature oxidation resistance, good electrical and thermal conductivities, thermal shock resistance, and wear resistance [13]. Moreover, they exhibit large plastic deformation at temperatures above 1200°C [14]. Since MAX phases also possess excellent irradiation/corrosion resistance, they are regarded as promising structural materials for fusion reactors and lead-cooled fast reactors [15]. Among all of the MAX phase materials, Ti_3SiC_2 has been considered a promising candidate structural material for nuclear and high-

temperature applications [8]. More recently, Ti_3SiC_2 has attracted considerable attention as a joining filler for SiC and CMC materials.

It is well known that Ti_3SiC_2 is the main phase formed when SiC is in a contact with Ti at high temperatures while $TiSi_2$ and TiC are secondary products [10, 16]. This in-situ formation of the Ti_3SiC_2 in the joining interlayer resulted in a relatively high 4-point bending strength when SiC was joined with Ti (100 MPa [17], 250 MPa [18], 126 MPa [4]). The formation of the Ti_3SiC_2 in the middle of the joined area was also observed when a Ti foil was used to join CMC materials [10]. While this reaction between Ti and SiC leads to an in-situ formation of a desirable Ti_3SiC_2 phase in the joining interlayer, rather high temperatures (1500°C [18], 1700°C [4, 10]) were required to obtain the joints. In order to decrease the joining temperature, joining of SiC or CMCs with Ti_3SiC_2 as a joining filler rather than its in-situ formation has been considered. However, in most of the works the joining procedures relied on the reaction between the joining filler and the matrix to obtain a strong joint. Either a pre-synthesized Ti_3SiC_2 powder [7] or Ti_3SiC_2 tapes [8] were used to join monolithic SiC materials using hot-pressing (HP) and SPS technologies at temperatures from 1300°C to 1600°C. In both cases, the flexural strength of the joined samples increased with increasing joining temperature, reaching maximum values of ~ 110 MPa and ~ 99 MPa for HP and SPS joining processes, respectively. In both these works, decomposition of Ti_3SiC_2 occurred at temperatures ≥ 1400°C, which was then followed by the chemical reaction with the SiC matrix. They concluded that the interface reactions were beneficial for obtaining sound joints as the lowest flexural strength was measured when no chemical reaction took place at 1300°C. A similar beneficial influence of the decomposition of Ti_3SiC_2 followed by the reactions with the matrix on the shear

strength of C_f/C composites was also reported [11]. In other words, although the Ti_3SiC_2 powders were used to join SiC and CMC materials, the best results were achieved when the amount of Ti_3SiC_2 decreased in the joining area due to both its partial decomposition and chemical reaction with SiC during joining.

On the contrary, in our recent work we demonstrated, for the first time, the advantages of the solid-state diffusion bonding over the solid-state reaction bonding when the pre-sintered Ti_3SiC_2 foil was used as a joining filler for the CVD-coated C_f/SiC and uncoated C_f/SiC, respectively [12]. In both cases, the sound joints were obtained using the SPS process at temperature as low as 1300°C, but the higher shear strength was measured when no reaction was found between the filler and the base material (~ 31 MPa vs. ~ 19 MPa for the coated and uncoated C_f/SiC composites, respectively).

Despite the fact that joining of SiC based ceramics has become an important issue for aerospace and nuclear applications (in both applications the operating in extreme conditions); there is the lack of information on the mechanical performance and thermal stability of the joints at high temperatures. Very recently, Dong et al. reported on the high temperature bending strength of the SiC joints with the Ti_3SiC_2 powder joined at 1400°C (up to 500°C in air) and Ti/Si/C/Al powder joined at 1600°C (up to 1200°C in air) [9]. While in the first case the overall poor strength of the joints (66 MPa; due to the porosity of the interlayer) significantly dropped to 21 MPa at 500°C, in the second case the strength first decreased from 133 MPa to 68 MPa at 800°C and then increased to 119 MPa at 1200°C. However, the impurities in the Ti_3SiC_2 filler and their oxidation led to the formation of TiO_2 that significantly affected the strength results. On the other hand, Jiménez et al. performed thermal cycle tests on SiC-C_f/SiC joints with Ti_3SiC_2

(also containing TiC and $TiSi_2$) under simulated re-entry conditions with respect to the envisaged applications, i.e. temperature profiles under vacuum [19]. Up to 5 cycles at two testing temperatures (1391°C and 1794°C) showed no detectable damage; instead the amount of Ti_3SiC_2 increased after the test as TiC reacted with $TiSi_2$. No other work on the high temperature stability and high temperature mechanical properties of the SiC based joints with Ti_3SiC_2 interlayer has been reported. Bulk Ti_3SiC_2 materials with different purities and microstructures were extensively investigated in the past and the high temperature mechanical properties of Ti_3SiC_2 are now well understood. However, it is not known whether its typical characteristics, such as brittle-ductile transformation at 1100-1200°C, very high plasticity above 1200°C, microcracks and cavity formation during deformation, etc., are retained when the Ti_3SiC_2 is constrained as the interlayer with a typical thickness up to ~ 100 μm between two ceramics. To the best of our knowledge, there has not been a reported systematic study on the high temperature stability and mechanical properties of monolithic CVD-SiC joints with high purity Ti_3SiC_2 interlayer (no unreacted TiC or TiC from decomposition of Ti_3SiC_2). The motivation for this work was to fill this gap and shed some light on the understanding of whether the Ti_3SiC_2 still keeps its characteristic of being a damage tolerant material with high plasticity even when confined as a layer in a SiC-SiC joint.

The aim of the present work was to develop a new joining technique for monolithic bulk CVD-SiC that would be appropriate for both aerospace and nuclear applications where the component geometry allows. Therefore, solid-state diffusion bonding at the temperature of 1300°C was applied using SPS. Based on our previous investigation on joining of CMCs [12], a pre-sintered highly pure

Ti_3SiC_2 foil was used as a joining filler to obtain a solid-state diffusion bonding. This is the first report on diffusion bonding of monolithic SiC materials when the Ti_3SiC_2 was used in the form of pre-sintered foils rather than powders [7, 9] or tapes [8]. The main advantage of such a solid-state diffusion bonding is that neither densification nor reaction is required to produce joints. This avoids the possibility of undesirable shrinkage of the joining interlayer as well as the volume change upon in-situ production of the reaction products. The joining conditions using SPS technology were carefully chosen to avoid both the decomposition of Ti_3SiC_2 and the reaction between the joining filler and the high purity CVD-SiC matrix. The bending strength of the joined components was then investigated at room as well as high temperatures up to 1400°C in vacuum. In addition, the creep resistance of the joints was studied in four point bending mode in the temperature range from 1000°C to 1200°C in vacuum. This work is the first study on the high temperature mechanical properties of the monolithic SiC materials joined with high purity Ti_3SiC_2 MAX phase (no TiC). This was done in order to determine the thermal stability of the joints in vacuum, thereby finding a potential temperature limit for the application of MAX phase interlayer as a joining filler.

2. Experimental procedure

2.1 Starting materials

The starting material was the high-purity (99.9995 %), fully dense (3.21 g/cm^3) CVD β-SiC (The Dow Chemical Company). The joining pairs of CVD-SiC blocks, rectangles with a dimension of 15 x 6 x 25 mm, were joined along the 15 x 6 mm cross-section. The surfaces to be joined were polished down using the final 1μm diamond paste.

Similar to our previous work on joining of CMCs [12], the thin foils used as a joining filler were pre-sintered from a synthesized Ti_3SiC_2 powder using the SPS process at 1300°C with an external pressure of 60 MPa and a dwell time of 5 min in vacuum. The Ti_3SiC_2 powder was synthesized from the elemental powders in the molar ratio of 1.0 Ti / 1.2 Si / 0.3 Al / 2.0 TiC in flowing argon at 1200°C for 2 hours; as described elsewhere [20]. The addition of Al for the synthesis of Ti_3SiC_2 was reported to significantly decrease the quantity of the TiC impurity in the final powder [20]. The Al added to the system also plays an important role of a deoxidation agent (by attracting the oxygen that is always present on the Ti powder), thereby promoting the formation of Ti_3SiC_2 phase and the densification of the compact [21]. Moreover, the presence of the in-situ formed Al_2O_3 (by the reaction between aluminum and oxygen) in the final Ti_3SiC_2 material was shown to improve the oxidation resistance as well as the hardness, strength and fracture toughness of Ti_3SiC_2 [20]. Therefore, aluminum was also used in this work to promote the purity, sintering and properties of the Ti_3SiC_2 phase. Hence, the final as-synthesized Ti_3SiC_2 powder contained a small amount of the intentionally added Al_2O_3 (~ 4.8 wt.%) and some impurities in the form of TiC and Ti_5Si_3. After the SPS sintering, the XRD analysis confirmed that the amount of impurities (TiC and Ti_5Si_3) was negligible, while the apparent amount of Al_2O_3 remained unchanged. More details about the pre-sintering of the Ti_3SiC_2 MAX phase foil using SPS, along with the XRD data for both the as-synthesized and the SPS pre-sintered Ti_3SiC_2, can be found in our previous work [12]. The pre-sintered Ti_3SiC_2 bulk samples were then ground to a final thickness of between ~ 30 and 100 μm and polished using a final diamond suspension of 3 μm. Afterwards, the foils were

cut into a rectangular shape to match the dimensions of the cross section of the CVD-SiC samples (15 x 6 mm). These foils were then used as the joining filler.

2.2 SPS joining process

The sketch of the joining setup is shown in Fig. 1. Before joining, the CVD-SiC blocks as well as the Ti_3SiC_2 foils were ultrasonically cleaned in acetone to remove any remaining dust particles, grease and other contaminants. The Ti_3SiC_2 foil was interposed between two CVD-SiC blocks as a sandwich and then inserted into a cylindrical graphite die with a diameter of 30 mm. The external pressure was applied through the graphite punches inserted in the cylindrical die. The graphite die was then wrapped in graphite felt to reduce heat loss. Both the die and the felt had a small hole enabling the temperature at the joining interface to be measured via a side-viewing infrared pyrometer. The joining assembly was indirectly heated to the joining temperature by the Joule heating of the graphite die in vacuum in an SPS furnace (HPD 25/1, FCT systems, Germany). The joining temperature was controlled using a top-viewing infrared pyrometer (measuring the temperature at ~ 2 mm from the sample top surface) while monitoring the temperature of the joining interface using the side-viewing optical pyrometer (see Fig. 1). The temperature difference measured using the top and side pyrometers was only ~ 50°C due to a uniform indirect heating via the graphite die. Therefore the joining temperature referred hereinafter is that

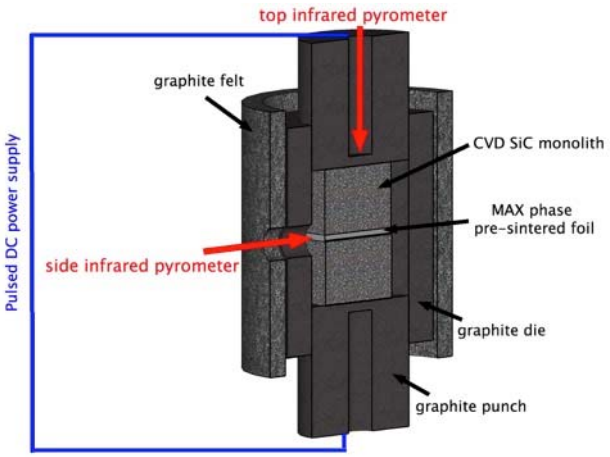

Fig. 1 Sketch of the SPS joining setup

measured by the top pyrometer. The joining temperature was carefully optimised to avoid reactions and decomposition to take place and final joints were obtained at 1300°C with an external pressure of 50 MPa. The heating and cooling rates were 100°C/min, while the holding time was 5 min.

2.3 Materials characterisation

After the joining, three beams with a dimension of 4 x 6 x 50 mm were cut out of each joined blocks along their long axis. Both edges on the tensile surfaces were chamfered by 45° in order to eliminate stress concentration. The tensile surfaces were polished up to using a final 1μm diamond suspension. The bending strength measurements were performed at room and high temperatures using the four point bending mode with the inner and outer spans of 20 and 40 mm, respectively. For the room temperature experiments, a universal electro mechanical testing machine (Instron 8862) equipped with a precision load cell calibrated to 5 kN force was used to apply loading. The cross-head speed was 0.5 mm/min and all room temperature tests were done in air. High temperature strength measurements were performed using a universal electro mechanical testing system (Messphysik-Zwick/Roel) equipped with a build-in vacuum furnace (MayTec) with Mo heating elements. The tests were performed in the temperature range between 1000°C and 1400°C in vacuum. The samples were preloaded to 20 N at room temperature and heated to the testing temperature with a heating rate of 10°C/min while maintaining the preload. After reaching the final testing temperatures, a dwell time of 15 min was used (to ensure temperature equilibrium) before applying a load with a cross-head speed of 0.5

mm/min until failure of the sample. A maximum force was obtained and used for the calculations of the strength values.

The same high temperature testing system was also used to perform creep studies in the temperature range of 1000 - 1200°C in vacuum. The same sample geometry and beam preparation as used for the high temperature strength tests was applied. Again, the samples were preloaded at room temperature in a four-point bending mode with the inner and outer spans of 20 and 40 mm, respectively. The samples were then heated to the testing temperature using Mo heating elements with a heating rate of 10°C/min in vacuum. A constant load of 200 N was applied after a 3 hours dwell at the testing temperatures (to ensure temperature equilibrium) until the failure of the samples (sudden drop of the applied load). The constant load was chosen to correspond to 50% of the average of all the maximum failure loads measured at 1200°C, and the same load was used for all testing temperatures. The deflection was recorded continuously during the loading in the centre of the inner span (middle of the samples) using a linear voltage differential transformer (LVDT). The minimum creep rates ($\dot{\varepsilon}$) were obtained as the slope of the secondary, steady-state, creep stage of the creep curve (strain vs. time). The apparent activation energy, Q, was determined by calculating the slope of a plot of $\log \dot{\varepsilon}$ versus 1/RT, according to the Arrhenius equation.

X-ray diffraction (XRD) patterns of Ti_3SiC_2 interlayer were obtained with an X-ray diffractometer (Siemens D5000 using Cu Kα radiation) on the as-joined sample as well as the fracture surfaces of the samples tested at high temperatures. The polished cross-sections of the joining areas and the fracture surfaces after the mechanical tests were characterized using Scanning Electron Microscopy (SEM) FEI Inspect-F equipped with Energy Dispersive Spectroscopy (EDS) detector.

Raman spectroscopy (RENISHAW) was used to investigate possible decomposition of the Ti_3SiC_2 interlayer on the tensile surfaces of the samples after the strength measurements at 1000°C and 1400°C. The sample surface was excited by a 633 nm laser fitted with an edge filter for Rayleigh line rejection and a CCD detector. The spectra (with an exposure time of 20 s and 3 accumulations) were obtained from three different areas using 20x and 100x objective lenses. The instrumental error associated with the Raman shift is 1 - 2 cm^{-1}.

3. Results and discussion

3.1 SEM analysis of the joints

Fig. 2 shows the backscattered SEM images of polished cross sections of the joints. Regardless the thickness of the initial pre-sintered foil (in the range of 30 – 100 μm), a uniform, homogenous and pores-free joining interface was obtained; see example in Fig. 2a. The SEM analysis showed that the joining interlayer well copied the polished surface of the CVD-SiC layer, filling up any small surface pores that remained after polishing; as highlighted by the arrows in Fig. 2b. Due to this conformal behaviour of the Ti_3SiC_2 foil, no pores, cracks or any visible defects were found along the CVD-SiC/Ti_3SiC_2 interfaces. In addition, no obvious reaction or transition layer was found at the interface between the Ti_3SiC_2 interlayer and the CVD β-SiC. Another important result of this work is that since the Ti_3SiC_2 foil did not melt, shrink or react with the CVD-SiC, the final thickness of joints was predetermined by the initial thickness of the Ti_3SiC_2 foil.

The microstructure of the Ti_3SiC_2 interlayer in the monolithic CVD SiC joints was found to be similar to the microstructure of the Ti_3SiC_2 interlayer in the case of CVD-SiC coated C_f/SiC joints reported in our previous work [12]. Fig. 2

shows that either plate-like or round Al_2O_3 grains (dark grey phase in the interlayer; shown as phase 2 in Fig. 2c) were homogenously distributed in the matrix of the Ti_3SiC_2 (shown as phase 1 in Fig. 2c). Their size varied from several hundreds of nanometers up to 6 μm. The microstructure of Ti_3SiC_2 consisted of the large laminated Ti_3SiC_2 grains and small equiaxial Ti_3SiC_2 grains. Similar to the case of joining of the CVD-SiC coated C_f/SiC with the Ti_3SiC_2 pre-sintered foil [12], an additional phase (shown as phase 3 in Fig. 2c) was also found in some small, well-separated areas in the interlayer. According to the EDS analysis (shown in [12]), this phase contained a significantly higher amount of Si than the Ti_3SiC_2 matrix while still containing a high amount of Ti. It is therefore believed that a small amount of titanium silicide was also present in the microstructure of the interlayer, despite the fact that it was not detected by the XRD analysis of the as-joined interlayer. This was due to the overall low content of titanium silicide in the interlayer (under the detection limit of XRD) and the fact that it was found in the small, well-separated areas. It should be noted here again that the XRD patterns for the as-synthesized as well as the as-sintered Ti_3SiC_2 were already reported in details in [12]. The XRD pattern of the interlayer after the joining process is shown later in Fig. 8, in comparison to the individual interlayers after the high temperature tests at different temperatures. As can be seen, the presence of titanium silicide was not detected in the interlayer after the joining.

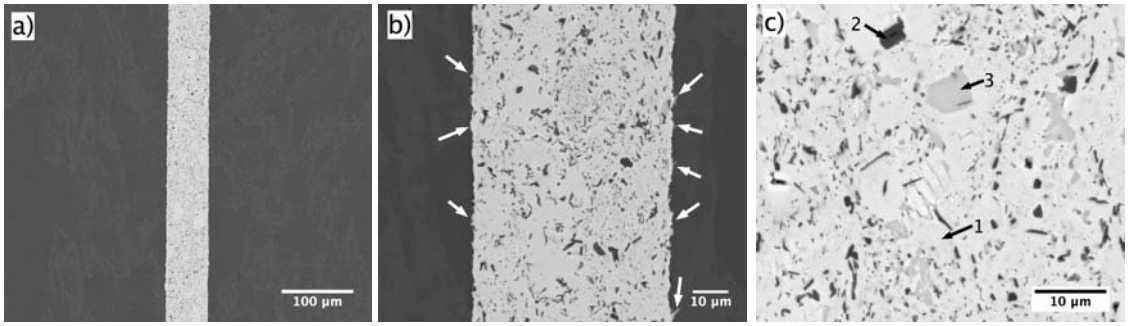

Fig. 2 Backscattered SEM images of the polished cross section of the CVD β-SiC joined with the pre-sintered Ti_3SiC_2 foil using SPS. Pores-free interface was observed with the joining material being infiltrated into the CVD-SiC surface pores (the arrows in b). Three phases can be distinguished in the microstructure of interlayer (figure c): 1 – Ti_3SiC_2, 2 – Al_2O_3, 3 – titanium silicide.

3.2 Bending strength of joints from room temperature up to 1400°C

The results of four-point bending strength of the joints investigated at different temperatures (22°C in air; from 1000°C to 1400°C in vacuum) are summarised in Fig. 3. The results for the individual samples along with the further information, such as thickness of the joining interfaces, failure initiation, and crack propagation, are given in Table 1.

The initial bending strength of the CVD β-SiC joints with the Ti_3SiC_2 pre-sintered interlayer (~ 220 MPa) did not deteriorate when tested at 1000°C in vacuum. The bending strength of the joints then linearly decreased with the increasing temperature above 1000°C (Fig. 3). This linear drop of strength is described by a linear regression function depicted in the graph. The joined components retained ~ 68% of their initial room temperature strength at 1200°C, while they retained ~ 38% of their initial strength at 1300°C (Table 1). The strength of the joined components significantly dropped at 1400°C at which two samples even failed at a preload of 20 N that corresponds to only ~ 7 MPa.

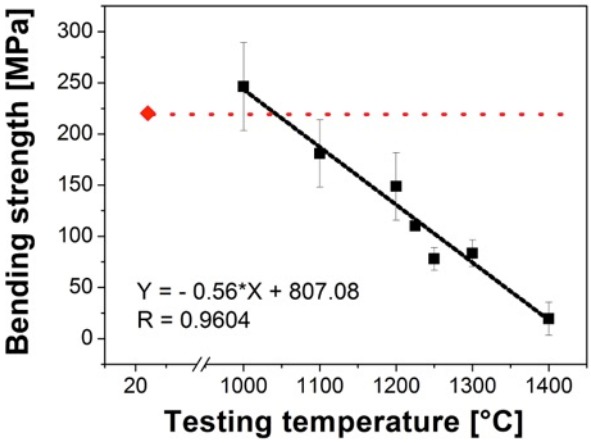

Fig. 3 Four-point bending strength of the CVD-SiC joints with the Ti_3SiC_2 pre-sintered interlayer measured at room temperature (22°C) in air and high temperatures (from 1000°C to 1400°C) in vacuum. The joined components retained ~ 68% of their initial strength when tested at 1200°C. The joining interlayer became the strength-limiting part of the joints at temperature above 1200°C.

Table 1 Summary of all bending strength results for individual samples measured at different temperatures, along with their joint thickness, and the location of the failure initiation and crack propagation.

Sample No.	**Joint thickness average ± SD [µm]**	**Testing temperature [°C]**	**Strength [MPa]**	**Strength average ± SD [MPa]**	**Failure initiation**	**Crack propagation**
1	32.7 ± 1.3		223.0		BM	BM
2	42.0 ± 2.8	22	216.7	220.3 ± 3.2	BM	BM
3	61.0 ± 2.4		221.3		BM	BM
4	48.3 ± 3.3		286.1		F	I+BM+F
5	54.8 ± 1.1	1000	252.0	246.3 ± 43.0	I/F	I+BM+F
6	99.9 ± 1.8		200.8		BM	BM
7	53.6 ± 1.7		163.1		I/F	I+F
8	62.1 ± 1.9	1100	160.8	180.9 ± 32.9	I	I+F+BM
9	87.0 ± 2.9		218.9		BM	BM
10	103.7 ± 1.2	1150	210.5	193.1 ± 24.5	BM	BM

11	63.3 ± 3.2		175.8		I	I+F+BM
12	31.9 ± 1.4	1200	135.7	148.8 ± 33.0	F	F+I
13	47.9 ± 4.5		97.5		F/I	F+I
14	50.7 ± 4.0		174.2		I-corner	I+F
15	91.2 ± 2.9		159.4		I	I+F+BM
16	99.0 ± 2.1		177.0		I/BM	I+BM+F
17	95.8 ± 2.6	1225	110.2	110.2	F/I	F+I
18	30.8 ± 0.7	1250	85.9	78.0 ± 11.2	F	F+I
19	92.3 ± 2.7		70.1		F	F+I
20	30.1 ± 1.0	1300	74.3	83.5 ± 13	F	F+I
21	49.9 ± 3.2		92.7		F	F
22	48.5 ± 3.5	1400	38.3	19.4 ± 16.3	F	F
23	76.1 ± 3.5		7*		F	F
24	87.2 ± 3.5		7*		I	I+F

I – interface; BM – base material; F – filler; * - materials failed at a preload (20 N), which corresponds to ~ 7 MPa; in the case of mixed crack propagation mode, the main crack path is always given as the first; SD – standard deviation.

As an example, different origins of failure and crack paths are shown in Fig. 4. At room temperature, the fracture origins (abnormal large SiC grains located very close to the tensile surface, or machining marks) were always found in the base CVD-SiC materials in the vicinity of the interface, and subsequently the cracks also propagated through the base materials (Fig. 4a). However, the location of the origin as well as the crack path changed with increasing temperature and moved towards the joining interlayer. In the temperature range of 1000 - 1200°C, the individual tested samples showed significantly different locations for the fracture origins (Table 1) and a complex mixed crack propagation (I+F+BM). This was

responsible for a significantly higher scatter of the strength values in this temperature range. Such a complex crack propagation is usually observed when the strength of the matrix, interface and joining interlayer are similar [8]. When the fracture origin was inside the joining filler (Fig. 4b), the highest bending strength (~ 286 MPa) among all of the measured values was recorded (Table 1). This suggests that the bending strength of this joint was predetermined by the strength of the filler. The value is in a good agreement with the four point bending strength of bulk Ti_3SiC_2 with a similar microstructure, which was reported to be ~ 300 MPa at ambient temperature [22]. This was the reason why a slightly higher average strength of the joints was measured at 1000°C when compared to the room temperature results (where the origin of failure was always in the base material). On the other hand, when the failure initiated and propagated in the base material, similar strength values were obtained at 1000°C, 1100°C and 1150°C in comparison with room temperature (see the values for the samples No. 6, 9, and 10 in Table 1). The interface between CVD-SiC and Ti_3SiC_2 played an important role at the temperature of 1100°C, 1150°C and 1200°C, as most of the fracture initiation sites were located at the SiC/Ti_3SiC_2 interface. In this temperature range, the crack propagated in a mixed mode, but in some cases almost complete delamination of the pre-sintered foil from the surface of CVD-SiC occurred (Fig. 4c). At testing temperatures ≥ 1200°C, no samples failed in the base material. The joining filler became the strength-limiting part of the joined components, and failure initiated and propagated solely in the filler at the temperatures above 1225°C (Fig. 4d).

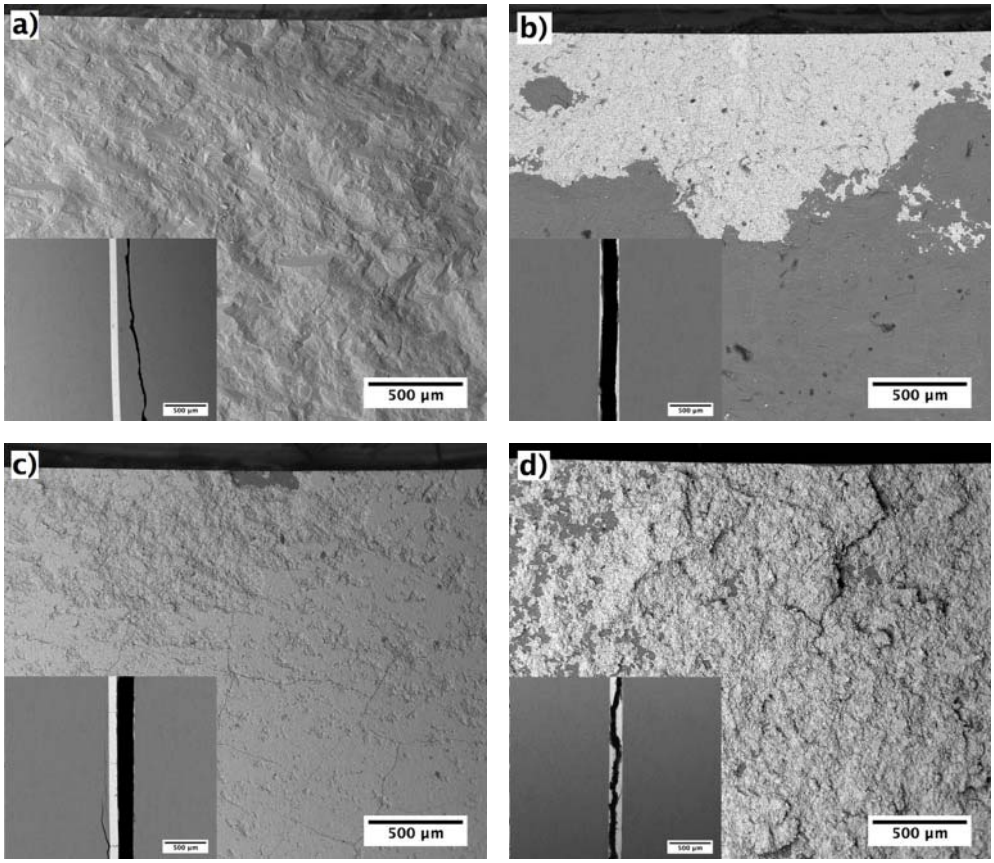

Fig. 4 Back-scattered SEM images of the fracture origins and crack propagation (inset images) revealed after four-point bending tests of the joined components: a) both the fracture origin and the crack path were located in the base CVD-SiC material, room temperature (sample No. 2); b) the fracture origin was inside the Ti_3SiC_2 joining filler and crack propagated in the filler and along the interface, 1000°C (sample No. 4); c) the fracture origin located at the interface or inside the filler while crack propagated solely along the interface; 1100°C (sample No. 7); d) both the fracture origin and the crack path were found in the filler; 1400°C (sample No. 22).

Another very important finding was that the bending strength of the joints appeared to be independent on the thickness of the Ti_3SiC_2 interlayer in the studied range from ~ 30 to 100 µm, see Table 1. The thickness of the interlayer varied from ~ 30 to ~ 60 µm when tested at room temperature, but very similar strength results within the scatter of ~ 3 MPa were obtained (all joined samples failed in the base material). Similarly, when the samples failed in the joining

interlayer at 1250°C, similar strength values were measured for the samples despite their significantly different joint thicknesses (~ 30 vs. ~ 90 μm).

The bending strength results of the joined components and the fractography analysis discussed above show that strong joints were obtained after solid-state diffusion bonding at temperature as low as 1300°C using SPS. In fact, the room temperature bending strength of the joined CVD-SiC was significantly higher when compared to the earlier works on joining of monolithic SiC with different forms of Ti_3SiC_2 (powders, or tapes) [7, 8, 9, 11]. When the Ti_3SiC_2 tapes were used to join monolithic SiC at different temperatures using SPS, the room temperature four-point bending strength varied from ~ 80 MPa to ~ 99 MPa [8]. The joints were stronger than the matrix (failure in the base material) only when joined at 1300°C, reaching a strength of ~ 80 MPa. A rather low strength value was attributed to the presence of porosity in the base material, as the SiC materials were pressureless sintered. The strength slightly increased with the increasing joining temperature and reached a maximum of 99 MPa at 1500°C. In this case, however, the joining interlayer began to decompose (presence of TiC, microcracks) and the fracture initiated in the joining filler. Similarly, Dong et al. reported that the monolithic pressureless SiC joints with a presynthesized Ti_3SiC_2 powder showed minimal room temperature bending strength (very close to zero!) when joined at 1300°C using SPS process [7]. The bending strength again increased with the increasing temperature, reaching maximum ~ 110 MPa for the joining temperature of 1600°C. The higher strength was attributed to the chemical reactions between the filler and the SiC matrix. However, decomposition of Ti_3SiC_2 in the joining temperature range of 1400-1600°C was again observed. The same authors also reported a maximum bending strength ~ 65 MPa when a Ti_3SiC_2

powder was used as a filler at a joining temperature of 1400°C, while a minimal strength of ~ 5 MPa was obtained for a joining temperature of 1300°C [9]. When they used 3Ti/1.2Si/2C/0.2Al powder as a joining filler, the bending strength increased with an increasing joining temperature, reaching maximum ~ 130 MPa when joined at 1600°C. The bending strength of ~ 50 MPa was measured for a component joined at 1300°C [9]. Though, in both cases the bending strength of the joints was far below the bending strength of the initial SiC monolithic materials (~ 360 MPa).

In the present work, high purity, fully dense CVD-SiC was successfully joined via solid-state diffusion bonding using a pre-sintered Ti_3SiC_2 foil at 1300°C, which led to the interface without presence of cracks or pores and any decomposition of the Ti_3SiC_2 filler. This was the reason why a significantly higher strength of the joined component was obtained when compared to the joints at the same joining temperature in the earlier works. In addition, the room temperature strength of the joints in this work was much higher than the strength of the components joined at higher temperatures [7, 8, 9]. Interestingly, the room temperature bending strength of the joints in the present work (~ 220 MPa) was also significantly higher when compared to the same CVD-SiC joined with Ti interlayer reported in our previous work (~ 126 MPa for the same geometry of testing samples) [4]. This is significant, as it shows that by replacing the Ti foil with the Ti_3SiC_2 pre-sintered foil the joining temperature of CVD-SiC could be significantly lowered (1300°C for Ti_3SiC_2 in this work vs. 1700°C for Ti [4]), while the strength of the joints significantly increased. A very good overall mechanical performance of the joined components can also be confirmed by the fact that the average bending strength of the joints at 1200°C (~ 148 MPa) was still higher than

all the room temperature strength values reported in the earlier works [4, 7, 8, 9]. The only previous work on the high temperature bending strength of the monolithic SiC joined with the Ti_3SiC_2 phase was done recently in air [9]. It showed that the overall poor strength of the joints in air (66 MPa) further dropped to 21 MPa at 500°C when Ti_3SiC_2 powder was used as the joining filler. Similarly, the strength of a monolithic SiC joined with Ti/Si/C/Al powder dropped from 133 MPa to 68 MPa at 800°C, and later increased with temperature as the results were affected by the oxidation. On the other hand, the joining technique used in the present work produced extraordinary strong SiC joints that retained ~ 70% of their initial room temperature strength at 1200°C, as shown above.

It is also important to point out that a small deviation from linearity was observed from the strain-stress curves (not shown here) for the samples tested at the temperatures above 1200°C. This deviation increased with increasing testing temperature. Since no systematic work has been reported on high temperature bending strength of SiC joints with Ti_3SiC_2 interlayer, it is interesting to look into the mechanical response of bulk Ti_3SiC_2 that was extensively investigated about a decade ago [13, 22, 23, 24, 26, 27]. Bulk Ti_3SiC_2 MAX phase exhibits a brittle-to-plastic transition at temperatures ~1100-1200°C at which point a large plastic deformation was obtained prior to failure [22, 23, 24, 26]. This transition can simply be detected by a deviation from linearity observed on the stress-strain curves. However, the stress at which non-linearity occurred during testing Ti_3SiC_2 bulk materials does not signify yield (activation of 5 independent slip systems), but it is the stress at which enough damage has accumulated in the material [23]. It was repeatedly observed that such high macroscopic strains (> 20%) result from the formation of pores in the form of cavities and microcracks, which are the

results of grain boundary sliding and decohesions [13, 23, 24, 26, 27]. Therefore, the maximum strain to failure that can be achieved in Ti_3SiC_2 is related to the linkage of the microcracks and cavities that form during deformation [23]. In other words, damage itself is responsible for the strain.

There are two possible reasons why a less significant deviation from the linearity of the stress-strain curves was observed in our work: 1) the limited volume of Ti_3SiC_2 that was confined as an interlayer between two SiC materials (with a thickness of 30-100 μm); 2) the rather high loading rate used. As regards the first point, it is hard to expect that such a thin interlayer (in the range of 30 - 100 μm) would cause a significant macro-plastic deformation of the whole joined assembly. Regarding the second point, Ti_3SiC_2 materials exhibit high strain-rate sensitivity [23]. This means that failure of the same Ti_3SiC_2, when tested at a particular high temperature, can be brittle or plastic for high and low strain rates, respectively. It was shown that at 1200°C Ti_3SiC_2 material exhibited brittle failure when loaded at a high rate (a cross-head speed of 0.1 mm/min), while it showed a significant plastic deformation (strain to failure of 22%) when a very slow loading rate (0.005 mm/min) was applied [23]. In the present work, even a higher loading rate was used (a cross-head speed of 0.5 mm/min), and combination of both reasons given above led to the fact that only a slight deviation from the linearity was detected from the strain-stress data.

As the small deviations from linearity in the stress-strain curves of the joints suggested, the same damage accumulation in the form of cavities and microcracks (reported for bulk Ti_3SiC_2) was also found in the Ti_3SiC_2 interlayer at high temperatures (above 1200°C). The formation of microcavities, as a result of grain boundary sliding and decohesion, became more significant at temperatures

≥ 1250°C, leading to the formation of microcracks that could be found on the tensile surface of the beams. As an example, Fig. 5a shows such a damage accumulation in the Ti_3SiC_2 joining material tested in bending at 1300°C in vacuum. The extensive formation of cavities, and grain boundary decohesion is highlighted in the circles. Grain boundary sliding and grain boundary decohesion accompanied by delamination along the basal planes were frequently observed. In good agreement with the present work, such a character of damage has been commonly observed during the high temperature testing of bulk Ti_3SiC_2 at temperatures above the brittle-to-plastic transition (~ 1100-1200°C) [22, 23, 24, 26]. It is believed that the linkage of the microcavities later resulted in the formation of microcracks (highlighted by the arrows in Fig. 5a) due to the increasing mechanical load. Once the microcracks had linked together, the major crack propagating through the middle of the joining interlayer caused the failure of the sample.

In addition, some plastically deformed large Ti_3SiC_2 grains could be found on the fracture surfaces of the joints tested at temperatures above 1250°C, see for example Fig. 5b. Polycrystalline Ti_3SiC_2 has a unique microstructure that contains many grains with hexagonal micro-lamellae. The planar boundaries between such lamellae are parallel to the basal planes of the crystal unit of Ti_3SiC_2 [22]. Fig. 5b shows delamination and slip or shear deformation of a single grain along the micro-lamellae boundaries, and these microlamellae were even slightly bent. With further deformation, the separated lamellae could deform by bending before rupturing [24]. Some holes could be seen that originated from slip between the micro-lamellae inside a coarse grain and pull-out of the micro-lamellae. All of this is the clear evidence of microplastic deformation. This behaviour is unusual for

non-metallic materials, but has been observed in Ti_3SiC_2 materials deformed at high temperatures [13, 24, 25]. Slip between the micro-lamellae inside a single grain was observed even at room temperature during four-point bending of Ti_3SiC_2 [22] or compression of Ti_3SiC_2 [25]. The hexagonal slices of micro-lamellae are weakly bonded (Van der Waals bonding) allowing easy shear slip. The kinking and delamination of individual grains together with intergranular fracture often accompany the deformation of polycrystalline Ti_3SiC_2. The kinks are usually accompanied by very sharp curvatures of the lamellae with acute angles as high as 60° [25]. However, a high plastic deformation of Ti_3SiC_2 was also observed without the evidence of kinking of the individual grains [23]. In the present work, no kinking of the micro-lamellae, and no micro-lamellae with such a high curvature were found. Instead, the delamination and a slight bending of the individual micro-lamellae of the Ti_3SiC_2 were observed in the interlayer. It is well known that the slip can occur in grains whose crystallographic orientation favours slip deformation. However, slip deformation is constrained at the grain boundaries, because the surrounding grains with different orientation hinder the advent of slip (due to the lack of 5 active slip systems to yield plastic deformation). The stress concentration accumulates at the points near the grain boundaries, finally leading to the initiation of microcracks [22, 24]. This is the only plausible mechanism to describe the high temperature bending deformation of the diffusion bonded CVD-SiC joints with the pre-sintered Ti_3SiC_2 foil. In conclusion, the same deformation mechanisms as observed during deformation of bulk Ti_3SiC_2 materials were identified in the temperature range of 1100 - 1400°C. In other words, the Ti_3SiC_2 interlayer with a thickness of 30-100μm retained the character

of a damage tolerant material, which is typical for bulk MAX phases as the ability to accumulate a significant level of damage before failure.

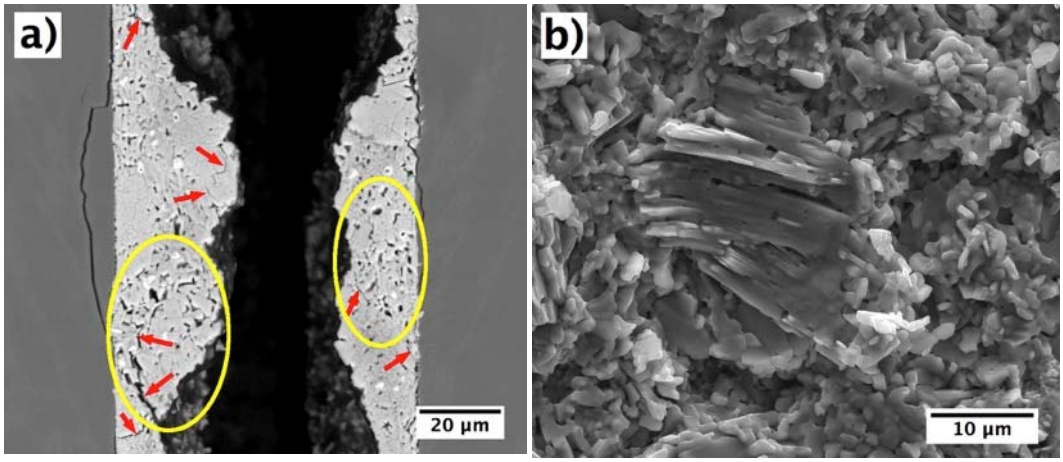

Fig. 5 a) Back-scattered SEM image of the tensile surface of the CVD-SiC joint with the Ti_3SiC_2 interlayer after four-point bending test at 1300°C in vacuum. Damage accumulation in the form of grain boundary sliding, decohesion and microcavities is highlighted in the circles. The arrows indicate the formation of microcracks. b) Fracture surface of the Ti_3SiC_2 interlayer after the bending test at 1300°C in vacuum, showing a heavily deformed large lamellar grain of Ti_3SiC_2. Sliding and bending of individual microlamellae and decohesion along their boundaries can be seen.

3.3 Creep resistance of the joints in the temperature range of 1000 - 1200°C

The results of the four-point bending creep resistance of the joints tested in the temperature range of 1000°C – 1200°C in vacuum are shown in Fig. 6a. All three typical regimes of creep deformation were observed at a constant load of 200 N, although the initial transient regime was minimal in all cases. The minimum creep rates were obtained from the secondary, steady-state, creep stage while the apparent activation energy was calculated assuming a power law relationship between the minimal creep rate, stress, and temperature [24]. The creep rate significantly increased by two orders of magnitude with the increasing

temperature from 1000°C to 1200°C, and the apparent activation energy was determined from the slope of the curve in Fig. 6b to be 521 ± 51 kJ.mol^{-1}. Since the minimum creep rate could be well described by the power law relationship (the high value for the coefficient of correlation, R = 0.972), it is assumed that the same thermally activated, rate-controlling mechanism(s) with the activation energy ~ 521 kJ.mol^{-1} operated over the entire investigated temperature range.

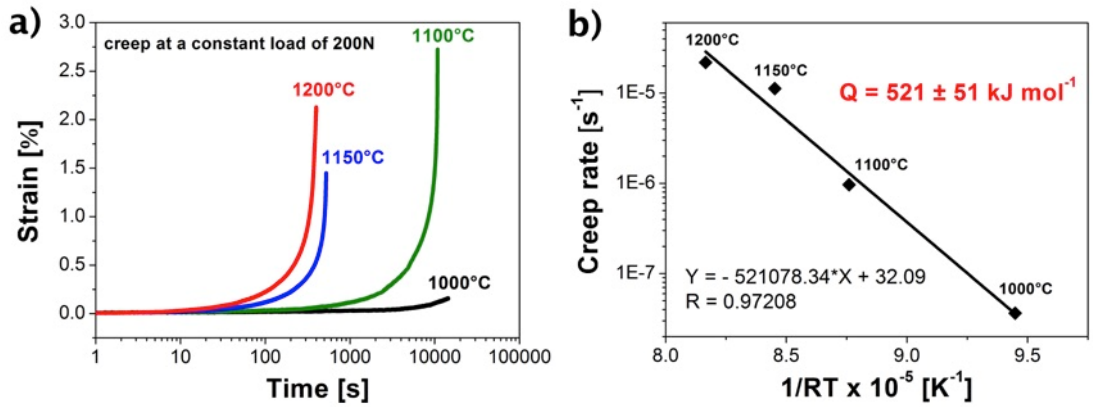

Fig. 6 a) Four-point creep resistance of the CVD-SiC joints with the Ti_3SiC_2 pre-sintered interlayer measured in the temperature range of 1000-1200°C at a constant load of 200N in vacuum until failure of the samples; b) Activation energy of the minimal creep deformation of the joints in the range of 1000-1200°C. As confirmed by the microstructural studies the joining filler was the creeping phase.

All the samples failed at the end of the third creep regime, which was accompanied by a sudden drop in the applying load. However, the samples investigated at 1000°C and 1200°C did not fall apart but the joined samples remained in one piece after the test, see Fig. 7a and 7d. The SEM analysis of the fracture surfaces (Fig. 7) revealed that all the samples failed in the joining area, as significant damage was observed after the tests in the joining interlayer while the CVD-SiC matrix was intact. Many small cavities and grain boundary decohesions

were found in all of the samples, regardless the testing temperature and time. The number of grain boundaries and triple-point cavities increased with time and temperature, and eventually coalesced into microcracks in a direction perpendicular to the maximum tensile load (indicated by the white arrows in Fig. 7). The rupture of the joined sample occurred when these microcracks linked into one major crack. The significant formation of microcracks was also found on the fracture surfaces of the individual samples that are shown in the insets in Fig. 7. The extent of microcracking significantly increased with the increasing testing temperature (see and compare all insets in Fig. 7). Most importantly, the formation of cavities and some initial stage of microcracking in the interlayer (highlighted by the red arrows in Fig. 7a) were also found for the sample tested at 1000°C. This clearly confirms (as suggested by the activation energy result above) that in the investigating temperature range the CVD-SiC joints deformed by the same creep mechanism(s), taking place in the Ti_3SiC_2 interlayer. In other words, the same damage accumulation in the Ti_3SiC_2 interlayer was observed as found during the high temperature bending strength measurements (grains sliding, grain boundary decohesions and cavities at grain boundaries), but the prolonged time during the creep enabled these locally deformed sites to link and form a significant number of microcraks with a wider opening. The fact that in some cases these microcracks did not propagate or connect to a long crack even at the testing temperature as high as 1200°C confirmed that the Ti_3SiC_2 interlayers could accumulate damage without a catastrophic failure. Such a damage tolerant character of bulk Ti_3SiC_2 was repeatedly observed during high temperature mechanical testing [13, 25, 26].

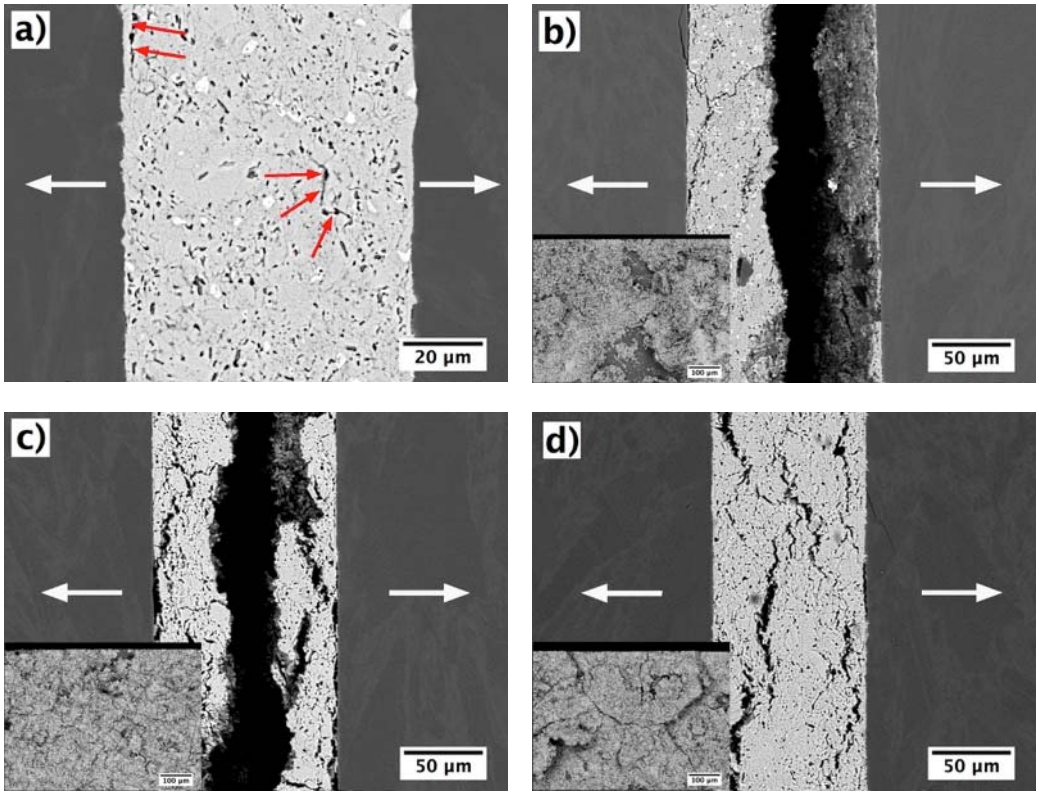

Fig. 7 Back-scattered SEM images of the tensile surfaces of the samples after the four-point bending creep test at a constant load of 200N: a) 1000°C; b) 1100°C; c) 1150°C; d) 1200°C. The white arrows indicate a direction of the maximal tensile stress. The fracture surfaces are shown as insets for the individual samples (the sample tested at 1000 did not fall apart despite a significant drop in the mechanical load).

It is well known that besides activation energy it is necessary to know a stress exponent (i.e. creep behaviour at different stresses) in order to understand the creep mechanism. Despite a detailed creep study was beyond the scope of this work, the present results show that the creep resistance of the joints was predetermined by the creep resistance of the Ti_3SiC_2 interlayer. Since no creep study has yet been conducted on the SiC joints with the Ti_3SiC_2 interlayer, it is worth comparing the present results with the ones obtained on the Ti_3SiC_2 bulk materials. It was reported that the response of the MAX phases to bending stresses is intermediate to that for compression and tension [13]. The activation

energy of the creep deformation of fine-grained bulk Ti_3SiC_2 materials was found to be ~ 445 kJ.mol^{-1} in the temperature range of 1000-1200°C [24] and ~ 537 kJ.mol^{-1} in a temperature range of 1100-1300°C [27] when measured in tension and compression, respectively. The activation energy of the creep deformation of the CVD-SiC joints with the 30-100 µm thick Ti_3SiC_2 interlayer (~ 521 kJ.mol^{-1}) is in the range of the previously reported values for bulk Ti_3SiC_2. Moreover, apparently the same formation of cavities, grain boundary decohesions, and microcracks were also found after the creep deformation of bulk materials. This is the same sign of damage accumulation in the material as usually occurs when Ti_3SiC_2 materials are exposed to the mechanical loads at high temperatures [13, 24]. Therefore the creep deformation of the joints can be explained as follows: during the primary creep stage, the slip of basal plane dislocations in the soft grains forms pile-ups at the grain boundaries, resulting in large internal stresses. The stress concentration accumulates at the grain boundary and the internal stresses could be accommodated by grain boundary cavitation and/or grain boundary sliding. Such a damage accumulation in the interlayer was also observed during the high temperature bending strength measurements in this work, as described in section 3.2. This became significant at higher temperatures, stresses and/or longer times, leading to a tertiary creep and finally causing the initiation of microcracks. Similar to the present work, it was also found that the ultimate failure in tension most probably occurred by the linking of smaller microcracks that ran perpendicular to the direction of the applied load [13].

3.4 Thermal stability/decomposition of the Ti_3SiC_2 interlayer

XRD pattern of the Ti_3SiC_2 interlayer in the as-joined samples, as well as XRD patterns of the interlayer adhered to the fracture surfaces after the bending tests at different temperatures are given in Fig. 8. Besides the major Ti_3SiC_2 phase (JCPDS # 01-089-1356), Al_2O_3 (JCPDS # 00-046-1212) was the only minor phase detected for the as-joined components. No other phases were detected by the XRD analysis. As mentioned in section 3.1, some well-separated areas of titanium silicides were found using back-scattered SEM analysis, however, their amount was apparently too low to be detected by the XRD. Decomposition of Ti_3SiC_2 materials has been extensively studied at different conditions (temperature, time, environment, atmosphere) and is now well understood that TiC_x is always a final product of decomposition [7, 13, 28, 29]. The absence of TiC_x in the joining interlayer indicates that initial high-purity Ti_3SiC_2 pre-sintered foil did not decompose during the joining process at the conditions applied (SPS, 1300°C, 50 MPa, 5 min). This is in good agreement with the other works reporting the decomposition of the Ti_3SiC_2 should not take place at temperatures ≤ 1300°C [7, 13, 28]. Similar to the present work, Dong et al. [7] showed that neither reaction nor decomposition took place when the monolithic SiC was joined with Ti_3SiC_2 powder using hot pressing at 1300°C with a holding time of 30 minutes. The reaction between the Ti_3SiC_2 interlayer and the SiC matrix as a result of the Ti_3SiC_2 decomposition followed by the reaction of the decomposition products with the matrix was reported to occur at joining temperatures > 1350°C [7, 8]. This all suggests that, as intended, the joining conditions were successfully selected in the present work to prevent a reaction between the Ti_3SiC_2 interlayer and the CVD β-SiC. Similarly, the present joining conditions did not lead to a decomposition of the Ti_3SiC_2, as no new phases were found in the interlayer after the joining.

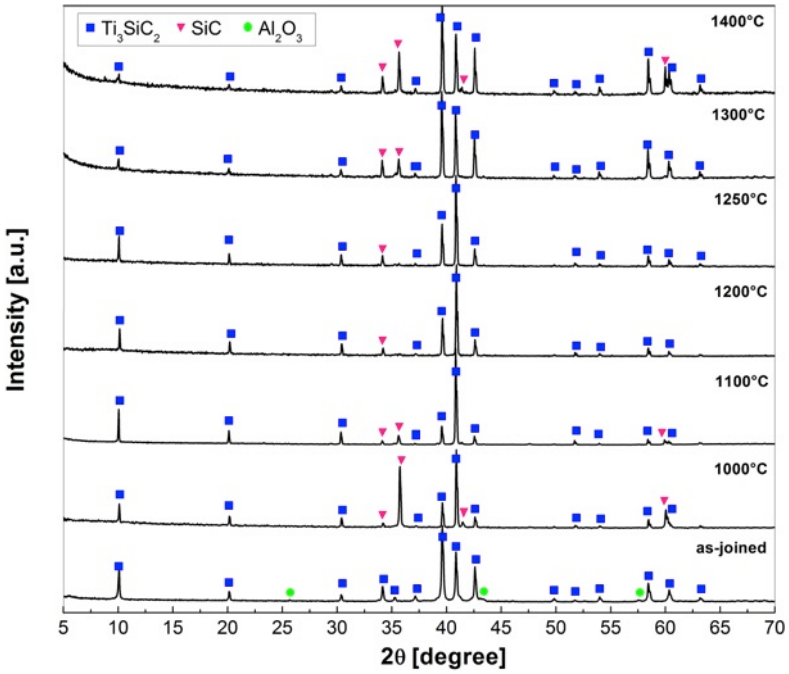

Fig. 8 XRD patterns of the Ti_3SiC_2 interlayer in the as-joined component and the fracture surface of the interlayer after high temperature bending strength measurements in vacuum. The presence of SiC is believed to come from the base SiC materials, as the patterns were taken from the interlayer adhered to the SiC on the fracture surfaces. No sign of Ti_3SiC_2 decomposition into TiC_x was found even at the maximum temperature of 1400°C. JCPDS cards No.: Ti_3SiC_2 (01-089-1356), Al_2O_3 (00-046-1212), SiC (01-075-0254).

More importantly, no additional phases in the interlayer were also detected on the fracture surfaces after the bending strength measurements at elevated temperatures. The only additional phase that appeared in all the XRD patterns were assigned to SiC (JCPDS # 01-075-0254), and this is believed to come from the base SiC materials as the data were recorded from the interlayer adhered to the SiC. The XRD analysis indicates that no decomposition of Ti_3SiC_2 occurred even during testing at temperatures as high as 1400°C in vacuum (this includes a

heating to the final temperature, an hour of holding time at the temperature plus the bending test itself).

In order to investigate the composition of Ti_3SiC_2 on the top surface of the interlayer (the area that can be seen in Fig. 5a as an example) rather than in its inner part on the fracture surfaces, Raman spectroscopy was used. The samples after bending strength tests at 1000°C and 1400°C were investigated. These were chosen as the representative of the conditions at which no decomposition would be expected (1000°C) and the highest investigated temperature (1400°C), at which decomposition might be expected. Ti_3SiC_2 has hexagonal structure with D_{6h}^{4} point group and P63/mmc space group. According to group theory, irreducible representation of the phonon optical modes for D_{6h}^{4} symmetry is Γ_{optic} = 2A1g + 3A2u + 3B1g + 3B2u + 6E2u + 6E2g + 6E1u + 4E1g. Among these modes only seven are Raman active: 2A1g + 2E1g + 3E2g [30]. The Raman spectra of the top surface of Ti_3SiC_2 interlayer after the bending strength tests at 1000°C and 1400°C are shown in Fig. 9. The following six Raman peaks at 135, 180, 224, 278, 625 and 676 cm^{-1} were assigned to Ti_3SiC_2. This is in good agreement with the Raman spectra of Ti_3SiC_2 reported before [31, 32]. No other Raman peaks were detected for the sample after the bending strength tests at 1000°C, Fig. 9.

On the other hand, some additional broad peaks at 374 and 431 cm^{-1} with a shoulder at 409 cm^{-1} were observed for the sample after the bending test at 1400°C, Fig. 9. These additional peaks were not found for the sample tested at the lower temperature, and were assigned to TiC_x ($x < 1$, carbon deficient) based on the earlier works [33, 34, 35]. According to similar trend of the peaks compared with those reported by Klein et al. [33], the position of the additional peaks

suggests that x was 0.97 or slightly lower in our work. However, a slight shift in the position of the TiC_x peaks in comparison with the earlier works on Raman spectroscopy of TiC is probably due to the different laser excitation sources and/or residual stresses and surrounding environment (the presence of the main Ti_3SiC_2 phase and not only TiC in this work). The other possible Raman peaks for TiC_x (reported to be around 600 cm^{-1} [33, 34, 35]) were probably superimposed on the main Ti_3SiC_2 phase. This was also observed in [31]. It is generally accepted that de-intercalation of Si from the structure triggers decomposition of Ti_3SiC_2. The low deficiency of carbon in TiC_x may indicate a mild decomposition of Ti_3SiC_2 as a result of insufficient removal of Si from the structure. The formation of intermediate product of $Ti_5Si_3C_x$ was not found in the present work. This all suggests a very small amount of TiC_x present in the Ti_3SiC_2 interlayer after the bending test at 1400°C. This means that during high temperature bending tests at 1400°C in vacuum there was a very mild decomposition of Ti_3SiC_2 interlayer into the TiC_x with a carbon deficiency of about 0.97. Such decomposition must have been in its early stage as no TiC_x was detected in the inner part of the interlayer (the fracture surface) either by XRD or Raman analysis.

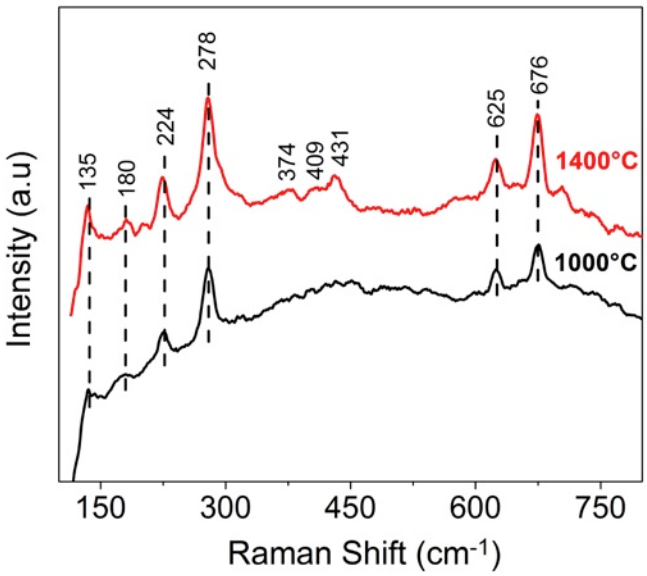

Fig. 9 Raman spectra of the tensile surface of the Ti_3SiC_2 interlayer after the bending strength measurements at 1000°C and 1400°C. The sample tested at 1400°C showed three additional peaks that were assigned to TiC_x.

The thermal stability of bulk Ti_3SiC_2 materials has been extensively investigated, but the results led to conflicting conclusions. El-Raghy et al. reported that Ti_3SiC_2 was stable for up to 24 h at 1600°C in vacuum and up to 4 h at 1600°C in argon [36]. Similarly, Radhakrishnan et al. showed that Ti_3SiC_2 was stable in a tungsten furnace for 10 h at 1600°C and 1800°C in argon, but significantly decomposed to TiC_x under the same conditions when heated in a graphite furnace [37]. On the other hand, Feng et al. reported that TiC_x was the only phase remaining on the surface of Ti_3SiC_2 after annealing at 1600°C for 2 h and 2000°C for 0.5 h in vacuum [38]. It was also reported that the surface of Ti_3SiC_2 started decomposing to form non-stoichiometric TiC and/or $Ti_5Si_3C_x$ at 1200°C in vacuum and completely decomposed at 1500°C [39]. Zeng et al. showed that the Ti_3SiC_2 started decomposing on the top surface after annealing for 1 h at a temperature as low as 1300°C in vacuum in a carbon-rich environment (graphite heating

elements, graphite plate), but was detectable in the inner bulk only after 1 h at 1400°C in vacuum [29]. It could be concluded that the stability of Ti_3SiC_2 is susceptible to the purity of materials, temperature, pressure and atmosphere (especially the vapour pressure of Si) [28]. Despite some contradictory results, it has now become essential knowledge that Ti_3SiC_2 materials are stable up to at least 1600°C in vacuum and at least 1800°C in argon, but their resistance to carburization appears to be poor [13].

Taking into account these contradictions in conditions at which Ti_3SiC_2 decomposes, it had been impossible to predict how the CVD-SiC joints with the Ti_3SiC_2 interlayer would have behaved under the testing conditions. In addition, it has to be pointed out that the mechanical loading at the high temperatures could have accelerated decomposition of the Ti_3SiC_2 interlayer. The present results confirm that the Ti_3SiC_2 interlayer was very stable up to 1300°C in vacuum during mechanical testing. After the mechanical tests at 1400°C, a very mild decomposition of the Ti_3SiC_2 interlayer was only detected by Raman spectroscopy (the presence of TiC_x) on the top surface while the inner part remained intact (no TiC_x detected on the cross section by either XRD or Raman analysis). Similarly, Zeng et al. also reported that the decomposition of Ti_3SiC_2 starts on the top surface and in its early stage it cannot be detected in the inner part [29]. Moreover, such a mild decomposition of Ti_3SiC_2 into TiC_x with a low carbon deficiency was very localized as the presence of TiC_x was only detected in some areas of the top surface of Ti_3SiC_2 by Raman spectroscopy using a 100x objective lens. It was also reported that the grain boundaries with flaws such as cracks or holes have lower threshold for the liberation of Si atoms, so the regions with flaws are the preferential positions for Si atoms to sublimate [29]. This may explain why the decomposition

was only found locally on the surface and also why this mild decomposition occurred at 1400°C in vacuum despite the fact that it was reported that under the right conditions the pure Ti_3SiC_2 is stable up to 1700°C [13]. The mechanical load at elevated temperatures resulted in grain boundary sliding, decohesions and the formation of microcavities and microcracks along the grain boundaries, as discussed above. This could have affected and accelerated the decomposition of Ti_3SiC_2 on the top surface, while the conditions were not severe enough for further decomposition towards the inner part of the interlayer. A maximum mechanical load located at the top tensile surface of the sample most probably accelerated the decomposition of the interlayer during high temperature bending.

Conclusions

The monolithic high purity CVD β-SiC materials were successfully joined with a pre-sintered Ti_3SiC_2 foil via solid-state diffusion bonding. No decomposition of Ti_3SiC_2 or reaction between the filler and the base material were observed after the joining at 1300°C/50 MPa/5 min using Spark Plasma Sintering.

For the first time, a systematic study of the high temperature properties of the CVD-SiC joints with Ti_3SiC_2 interlayer in vacuum is reported. The initial bending strength of the joints (~ 220 MPa) did not deteriorate when tested at 1000°C in vacuum. The bending strength of the joints then linearly decreased with the increasing temperature above 1000°C. The joined components retained 68% of their initial bending strength at 1200°C in vacuum, while they retained ~ 38% of their initial strength at 1300°C. The strength of the joined components significantly dropped to an average of ~ 19 MPa at 1400°C in vacuum. At the testing temperatures ≥ 1200°C, no samples failed in the base material and the

joining filler became the strength-limiting part of the joined components. The Ti_3SiC_2 interlayer with a thickness of 30-100μm retained the character of a damage tolerant material, which is typical for bulk MAX phases, with the ability to accumulate a significant level of damage before failure. This included grain boundary sliding and decohesion, and the formation of cavities at the grain boundaries and the subsequent formation of microcracks. Moreover, the large Ti_3SiC_2 grains showed some plastic deformation in the form of micro-lamellae sliding, delamination and bending.

The activation energy of the creep deformation in the temperature range of 1000-1200°C in vacuum was ~ 521 $kJ.mol^{-1}$. The minimum creep rate significantly increased by two orders of magnitude when the temperature increased from 1000°C to 1200°C. All of the creep deformation was localized in the interlayer as no damage to the base CVD-SiC was detected. Again, a significant ability to accumulate damage was observed. The formation a significant number of microcracks with wide openings that subsequently linked to a major crack was responsible for the failure of the materials.

The Ti_3SiC_2 joining interlayer was found to be stable up to 1300°C in vacuum during mechanical testing. A mild and well-localized decomposition of Ti_3SiC_2 to TiC_x was found by Raman spectroscopy on the top surface of the interlayer after mechanical test at 1400°C in vacuum, while the inner part remained intact (proved by both XRD and Raman analysis). A maximum mechanical load located at the top tensile surface of the sample may have accelerated the decomposition of the interlayer during high temperature bending.

Acknowledgement

The research leading to these results has received funding from the European Community's 7th Framework Programme FP7 2007-2013 under the grant agreement n. 609188, within the European project ADMACOM (Advanced manufacturing routes for metal/composite components for aerospace).

References

1. M. C. Halbig, M. Singh, T. P. Shpargel, J. D. Kiser (2006) Diffusion bonding of silicon carbide ceramics using titanium interlayers, in Mechanical properties and performance of engineering ceramics II: Ceramic Engineering and Science Proceedings, Volume 27, Issue 2 (eds R. Tandon, A. Wereszczak and E. Lara-Curzio), John Wiley & Sons, Inc., Hoboken, NJ, USA.
2. L. L. Snead, T. Nozawa, Y. Katoh, T. S. Byun, S. Kondo, D. A. Petti, Handbook of SiC properties for fuel performance modelling, J. Nucl. Mater. 371 (2007) 329-377.
3. Y. Katoh, L. L. Snead, T. Cheng, C. Shih, W. D. Lewis, T. Koyanagi, T. Hinoki, C. H. Henager Jr., M. Ferraris, Radiation-tolerant joining technologies for silicon carbide ceramics and composites, J. Nucl. Mater. 448 (2014) 497-511.
4. S. Grasso, P. Tatarko, S. Rizzo, C. Hu, Y. Katoh, M. Salvo, M. J. Reece, M. Ferraris, Joining of β-SiC by spark plasma sintering, J. Eur. Ceram. Soc. 34 (2014) 1681-1686.
5. B. V. Cockeram, Fracture toughness and flexural strength of chemically vapor-deposited silicon carbide as determined using chevron-notched

and surface crack in flexure specimens, J Am Ceram Soc 87[6] (2004) 1093-1101.

6. Y.-II Jung, J.H. Park, H.G. Kim, D.J Park, J.Y. Park, W.J. Kim, Effect of Ti and Si interlayer materials on the joining of SiC ceramics, Nucl. Eng. Tech. (2016) in press, http://dx.doi.org/10.1016/j.net.2016.03.001
7. H. Dong, S. Li, Y. Teng, W. Ma, Joining of SiC ceramic-based materials with ternary carbide Ti_3SiC_2, Mat. Sci. Eng. B 176 (2011) 60-64.
8. X. Zhou, Y. H. Han, X. Shen, S. Du, J. Lee, Q. Huang, Fast joining SiC ceramics with Ti_3SiC_2 tape film by electric field-assisted sintering technology, J. Nucl. Mater. 466 (2015) 322-327.
9. H. Dong, Y. Yu, X. Jin, X. Tian, W. He, W. Ma, Microstructure and mechanical properties of SiC-SiC joints joined by spark plasma sintering, Ceram. Int. 42 (2016) 14463-14468.
10. S. Rizzo, S. Grasso, M. Salvo, V. Casalegno, M.J. Reece, M. Ferraris, Joining of C/SiC composites by spark plasma sintering, J. Eur. Ceram. Soc. 34 (2014) 903-913.
11. X. Zhou, H. Yang, F. Chen, Y.-H. Han, J. Lee, S. Du, Q. Huang, Joining of carbon fiber reinforced carbon composites with Ti_3SiC_2 tape film by electric field assisted sintering technique, Carbon 102 (2016) 106-115.
12. P. Tatarko, V. Casalegno, C. Hu, M. Salvo, M. Ferraris, M.J. Reece, Joining of CVD-SiC coated and uncoated fibre reinforced ceramic matrix composites with pre-sintered Ti_3SiC_2 MAX phase using Spark Plasma Sintering, J. Eur. Ceram. Soc. (2016) in press, http://dx.doi.org/10.1016/j.jeurceramsoc.2016.06.025

13. M. W. Barsoum (2013) MAX phases: properties of machinable ternary carbides and nitrides, Wiley-VCH Verlag GmbH & Co. KGaA, Germany; ISBN: 978-3-527-33011-9.
14. T. El-Raghy, M.W. Barsoum, A. Zavaliangos, S.R. Kalidindi, Processing and mechanical properties of Ti_3SiC_2: II, Effect of grain size and deformation teperature, J. Am. Ceram. Soc. 82[10] (1999) 2855-2860.
15. F. Li, H. Zhang, Q. Wang, D. Qu, T. Zhou, B. Kim, Y. Sakka, C. Hu, Q. Huang, Microwave sintering of $Ti_3Si(Al)C_2$ ceramic, J. Am. Ceram. Soc. 97[9] (2014) 2731-2735.
16. B. Gottselig, E. Gyarmati, A. Naoumidis, H. Nickel, Joining of ceramics demonstrated by the example of SiC/Ti, J. Eur. Ceram. Soc. 6 (1990) 153-60.
17. S. Morozumi, M. Endo, M. Kikuchi, K. Hamajima, Bonding mechanism between silicon carbide and thin foils of reactive metals, J. Mater. Sci. 20 (1985) 3976-3982.
18. M. Naka, J. C. Feng, J. C. Schuster, Phase reaction and diffusion path of the SiC/Ti system, Metall. Mater. Trans. A 28 (1997) 1385-1390.
19. C. Jiménez, K. Mergia, M. Lagos, P. Yialouris, I. Agote, V. Liedtke, S. Messoloras, Y. Panayiotatos, E. Padovano, C. Badini, C. Wilhelmi, J. Barcena, Joining of ceramic matrix composites to high temperature ceramics for thermal protection systems, J. Eur. Ceram. Soc. 36 (2016) 443-449.
20. K. Sato, M. Mishra, H. Hirano, C. Hu, Y. Sakka, Pressureless sintering and reaction mechanism of Ti_3SiC_2 ceramics, J. Am. Ceram. Soc. 97[5] (2014) 1407-1412.

21. Z. M. Sun, Y. Zou, S. Tada, H. Hashimoto, Effect of Al addition on pressureless reactive sintering of Ti3SiC2, Scripta Mater. 55 (2006) 1011-1014.
22. J. F. Li, W. Pan, F. Sato, R. Watanabe, Mechanical properties of polycrystalline Ti_3SiC_2 at ambient and elevated temperatures, Acta Mater. 49 (2001) 937-945.
23. M. Radovic, M.W. Barsoum, T.EL-Raghy, J. Seidensticker, S. Wiederhorn, Tensile properties of Ti_3SiC_2 in the 25-1300°C temperature range, Acta Mater. 48 (2000) 453-459.
24. M. Radovic, M.W. Barsoum, T. El-Raghy, S.M. Wiederhorn, Tensile creep of coarse-grained Ti_3SiC_2 in the 1000-1200°C temperature range, J. Alloy Compd. 361 (2003) 299-312.
25. Y. Zhou, Z. Sun, Micro-scale plastic deformation of polycrystalline Ti_3SiC_2 under room-temperature compression, J. Eur. Ceram. Soc. 21 (2001) 1007-1011.
26. Z.F. Zhang, Z.M. Sun, H. Hashimoto, Deformation and fracture behavior of ternary compound Ti_3SiC_2 at 25-1300°C, Mater. Lett. 57 (2003) 1295-1299.
27. T. Zhen, M.W. Barsoum, S.R. Kalindindi, M. Radovic, Z.M. Sun, T. El-Raghy, Compressive creep of fine and coarse-grained Ti_3SiC_2 in air in the 1100-1300°C temperature range, Acta Mater. 53 (2005) 4963-4973.
28. N. F. Gao, Y. Miyamoto, D. Zhang, On physical and thermomechanical properties of high-purity Ti_3SiC_2, Mater. Lett. 55 (2002) 61-66.

29. J. Zeng, S. Ren, J. Lu: Phase evolution of Ti_3SiC_2 annealing in vacuum at elevated temperatures, Int. J. Appl. Ceram. Technol. 10[3] (2013) 527-539.
30. Bilbao crystallographic server. URL: "http://www.cryst.ehu.es/rep/sam.html", 25/07/2016.
31. M. Amer, M.W. Barsoum, T. El-Raghy, I. Weiss, S. Leclair, D. Liptak, The raman spectrum of Ti_3SiC_2, J. Appl. Phys. 84[10] (1998) 5817-5819.
32. F. Mercier, O. Chaix-Pluchery, T. Ouisse, D. Chaussende, Raman scattering from Ti_3SiC_2 single crystals, Appl. Phys. Lett. 98 (2011) 081912.
33. M. V. Klein, J. A. Holy, W. S. Williams, Raman scattering induced by carbon vacancies in TiC_x, Phys. Rev. B 17[4] (1978) 1546-1556.
34. K. J. Cai, Y. Zheng, P. Shen, S. Y. Chen, TiC_x-Ti_2C nanocrystals and epitaxial graphene-based lamellae by pulsed laser ablation of bulk TiC in vacuum, Cryst. Eng. Comm. 16 (2014) 5466-5474.
35. P. Zhang, T. L. Ngai, Z. Ding, Y. Li, Erosion craters on Ti_3SiC_2 anode, Phys. Lett. A 378 (2014) 2417-2422.
36. T. El-Raghy, M. W. Barsoum, Processing and mechanical properties of Ti_3SiC_2: I, Reaction path and microstructure evolution, J. Am. Ceram. Soc. 82[10] (1999) 2849-2854.
37. R. Radhakrishnan, J. J. Williams, M. Akinc, Synthesis and high-temperature stability of Ti_3SiC_2, J. Alloys Compd. 285 (1999) 85-88.
38. A. Feng, T. Orling, Z. A. Munir, Field-activated pressure-assisted combustion synthesis of polycrystalline Ti_3SiC_2, J. Mater. Res. 14 (1999) 925-939.

39. I. M. Low, Depth profiling of phase composition in a novel Ti_3SiC_2 -TiC system with graded interfaces, Mater. Lett. 58 (2004) 927-932.